Article

Journal of Vibration and Control
2020, Vol. 26(23–24) 2174–2184

DOI: 10.1177/1077546320915333
journals.sagepub.com/home/jvc
SAGE

Three degrees of freedom rotary double inverted pendulum stabilization by using robust generalized dynamic inversion control: Design and experiments

Ibrahim M Mehedi[1,2], Uzair Ansari[2] and Ubaid M AL-Saggaf[1,2]

Abstract

The aim of this article was to determine control strategy for balance control of rotary double inverted pendulum system, which is highly nonlinear and unstable under-actuated system. The complexities involved in rotary double inverted pendulum dynamics make this system a useful engineering test bed to test and verify newly designed controllers. In this article, a constraint-based control approach titled robust generalized dynamic inversion is designed and implemented for robust stabilization of rotary double inverted pendulum system. The robust generalized dynamic inversion control is designed in two stages; in the first stage, constraint differential equations of the controlled state variables are prescribed, which encompasses the control objectives. To enforce the constraint dynamics, the equivalent control is realized by means of Moore–Penrose generalized inversion. To enhance robustness, the switching (discontinuous) control is introduced in second stage, whose design principle is based on classical sliding mode control theory. Finally, the controllers obtained in two stages are augmented to form the resultant robust generalized dynamic inversion control law. The proposed controller ensures robustness along with improved time domain performance regardless of system nonlinearities, uncertainties, and unwanted disturbances. The stability analysis is presented for guaranteeing semi-global asymptotically stable closed loop performance via Lyapunov stability criteria. Numerical simulation and experimental investigations are carried out along with comparative analysis, to demonstrate the effectiveness of robust generalized dynamic inversion control algorithm over other conventional control methods.

Keywords

Rotary double inverted pendulum, robust generalized dynamic inversion, sliding mode control, Lyapunov stability, robust control

1. Introduction

Rotary single inverted pendulum and rotary double inverted pendulum (RDIP) are the most common type of pendulum systems found in control laboratories (Singh and Yadav, 2012). RDIP system consists of a horizontal arm driven by dc motor with two unstable pendulum links. The system has number of actuators lesser than the degrees of freedom, which makes it highly under-actuated. Because of the typical configuration of RDIP system, it is a challenging task for the engineers to design suitable controllers to stabilize it.

Several investigations are available in literature proposing linear and nonlinear control strategies for stabilization of the RDIP system. Among linear control approaches, linear quadratic regulator (LQR) is the most common method which needs sufficient knowledge of system dynamics to achieve stable performance. In Yadav et al. (2012), the authors have implemented LQR control by estimating the system parameters at which the controller gives optimized performance for stabilizing the RDIP system.

As an alternative, research work have been conducted in literature by exploring and implementing modern nonlinear

[1]Department of Electrical and Computer Engineering (ECE), King Abdulaziz University, Saudi Arabia
[2]Center of Excellence in Intelligent Engineering Systems (CEIES), King Abdulaziz University, Saudi Arabia

Received: 11 October 2019; accepted: 5 March 2020

Corresponding author:
Ibrahim M Mehedi, Department of Electrical and Computer Engineering (ECE), Center of Excellence in Intelligent Engineering Systems (CEIES), King Abdulaziz University, Jamea, Jeddah 21589, Saudi Arabia.
Email: imehedi@kau.edu.sa

control approaches to control complex RDIP system. The authors have investigated linear matrix inequalities in Hoang and Wongsaisuwan (2007) by implementing H_∞ control to deal with the problems which are robustness and minimization problem. The proposed method stabilize the RDIP system regardless of certain parametric uncertainties and input disturbances. Back stepping control for the under-actuated RDIP system is described by Jabbar et al. (2017), where in the first stage, the controller is implemented for individual active and passive links, and in the second stage, a Lyapunov-based compensator is designed to cater uncertain terms for individual link. The design and implementation of fractional order controller (FOC) investigated by Mehedi et al. (2019) for controlling RDIP system is a promising research domain. The controller offers improved tracking performance and more flexibility in parameters tuning as compared with classical integer order controllers. The authors in Dabiri et al. (2016) presented the fuzzy logic controller with destabilizing fractional dampers for the RDIP system in the presence of uncertainties. In the proposed method, the linguistic rules depend on the qualitative motion of the passive pendulum links, which stabilize the RDIP system at unstable equilibrium point. The problem of optimal control of the RDIP system is addressed in Nejadfard et al. (2013), where neuro-fuzzy strategy is applied to construct the inverse model of friction dynamics, which improves the steady state response significantly.

On the other hand, the sliding mode control (SMC) is popular by virtue of its invariance characteristic to parametric uncertainties, system nonlinearities, and disturbance rejection. In Patil and Kurode (2017), the performance of SMC is demonstrated through numerical simulations and experimental investigations of RDIP system. Another control technique, nonlinear dynamic inversion (NDI), is famous for its feedback linearization method by unwrapping a complex nonlinear system into a simpler linear system, which allows linear control methods to achieve control objectives. The results presented in Young et al. (2006), demonstrate the control of the RDIP system numerically by using NDI with the timescale separation principle. Beside these advantages, the methodology has certain shortcomings by virtue of blind cancellation of useful nonlinearities, requirements for finding exact mathematical model of the system, assumptions required to find its inverse model, square dimensionality restriction, etc.

On the contrary, a nonlinear technique called generalized dynamic inversion (GDI) is emerging as a novel inversion-based control law, where control objectives are defined in the form of constraint differential equations (Mehedi et al., 2018). The virtual constraint dynamics are formulated as the function of controlled state variable deviation functions, which are evaluated along the solution trajectories of the dynamical system. The control law is realized by engaging Moore–Penrose generalized inverse (MPGI) (Moore, 1920; Penrose, 1955). The resultant GDI control expression has two components, one is the particular part that enforces the constraint dynamics and other one is the null control vector that has a portion in the null-space of the controls coefficient. The classical GDI is being updated progressively over the years by including robust and adaptive attributes to provide robustness and to achieve improved tracking performance (Ansari and Bajodah, 2018a, 2019; Ansari et al., 2018, 2019a).

The tracking and stabilization problem of RDIP system is addressed in this article through robust generalized dynamic inversion (RGDI) control, which comprises of equivalent and switching control terms. The equivalent control (conventional GDI) is constructed by prescribing virtual constraint dynamics in the form of three ordinary differential equations. The three constraint equations are construction based on the function of angular position errors of horizontal rotary arm and the two pendulum links, respectively. The equivalent control is realized by inverting the constraint differential equations by engaging MPGI. Because the system under consideration is highly unstable, it is crucial to augment some robustness. This is accomplished by integrating a discontinuous term based on the principle of SMC, which provides robustness along with improved tracking performance and faster convergence (Ansari and Bajodah, 2017). The convergence analysis of the closed loop system will guarantee semi-global asymptotically stable tracking performance in the sense of Lyapunov by constructing a positive definite Lyapunov candidate function.

Specific to the RDIP system stabilization problem, the proposed RGDI control is not benefited by the privilege of null control vector that provides extra degree of control design freedom (Ansari and Bajodah, 2018b). This is because of the under-determined nature of constraint differential equations, that is lesser control variables than the number of constraint equations. However, this deficiency has been addressed intelligently by augmenting the switching control term for improving the tracking performance.

The proposed RGDI control has several advantages over other algorithms available in literature. The RGDI control is of left inversion type; therefore, it overcomes the drawbacks of NDI, as it does not involve the complications required to find the inverse model of plant dynamics as well as blind cancellation of favourable system nonlinearities. Furthermore, the augmentation of discontinuous term based on sliding mode approach will allow the inclusion of robust attributes along with improved tracking performance, when the system is under influence of uncertain dynamics, system nonlinearities, and external perturbations.

The contribution of this article to the control theory is twofold, that is analytical and empirical. Theoretically, the RGDI control is designed and implemented to stabilize the under-actuated RDIP system. On the experimental side, the controller performance is evaluated rigorously through computer simulations and by performing experiments on

the benchmark Quanser's RDIP test bed to investigate real time performance. Furthermore, the superiority of experimental results obtained by the RGDI algorithm is justified through comparisons with conventional SMC and FOC strategies.

2. RDIP mathematical modeling

This section presents the mathematical modeling of the RDIP system developed by Quanser (2012), whose dynamics is depicted schematically in Figure 1, which is similar to a two-link robotic arm. The system under consideration consists of a dual pendulum links mounted by hinge on the horizontal rotary arm. The control torque provided by the horizontal rotary arm actuates and stabilizes the two pendulum links via the gear transmission system. The angular position feedbacks of the rotary arm, that is θ and the pendulum link angles α and ϕ are sensed by the three encoders mounted at the arm shaft and the hinge points of the pendulum links, respectively. Different parts of the schematic shown in Figure 1 are labeled to understand the dynamics of the RDIP system. The length of the rotary arm is denoted by L_r, J_r is the moment of inertia and θ is the rotating angle. The length of pendulum links are represented by L_{p1} and L_{p2}, l_{p1} and l_{p2} are their center of mass, J_{p1} and J_{p2} are the moment of inertia, and M_{p1} and M_{p2} are their masses. The deflection angles of pendulum 1 and 2 are denoted by α and ϕ, respectively. For more accuracy, the mass of hinge between pendulum links is also taken into consideration, which is denoted by M_h in calculations. The major design parameters along with their numerical values of Quanser RDIP system are given in Table 1 (see Quanser (2009, 2012)).

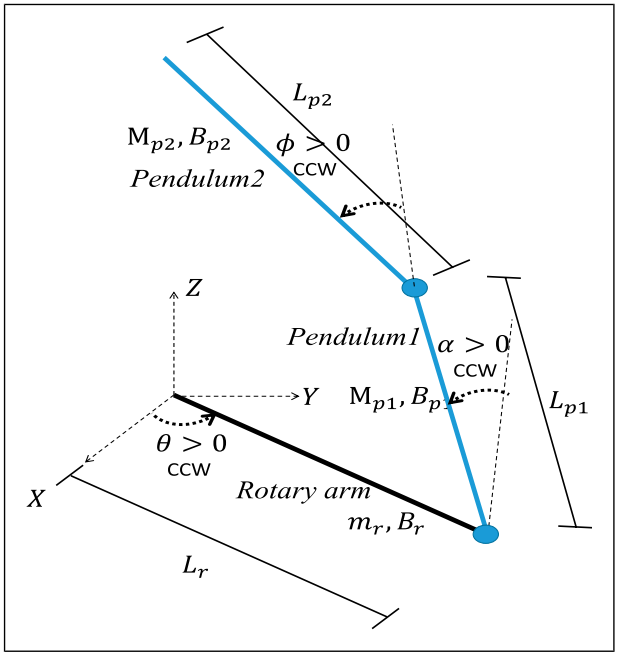

Figure 1. Schematic diagram of rotary double inverted pendulum system.

2.1. Nonlinear dynamics of RDIP

Instead of classical mechanics, RDIP dynamics which relates the motions of the horizontal rotary arm and the two pendulum links with respect to the servo motor voltage is derived using the Lagrange equation of motion, resulting in

$$\frac{\partial^2 L}{\partial t \partial \dot{q}} - \frac{\partial L}{\partial q} = Q \tag{1}$$

where vector q represents generalized coordinates and expressed as

$$q(t)^T = [\theta(t) \quad \alpha(t) \quad \phi(t)] \tag{2}$$

and the corresponding velocity vector is described as

$$\dot{q}(t)^T = \left[\frac{\partial \theta(t)}{\partial t} \quad \frac{\partial \alpha(t)}{\partial t} \quad \frac{\partial \phi(t)}{\partial t}\right] \tag{3}$$

where L is the Lagrangian of the system and it is written as

$$L = T - V \tag{4}$$

where T is the total kinetic energy and V is the potential energy of the system. The total kinetic energy is defined as the summation of kinetic energies of bottom pendulum link, rotary arm, hinge, and top pendulum link and is described as

$$T = T_b + T_r + T_h + T_t \tag{5}$$

where T_b represents kinetic energy of lower pendulum link, T_r is kinetic energy for rotary arm, kinetic energy for hinge point is denoted by T_h, and T_t is the kinetic energy of upper pendulum link, whose details are found in Quanser (2012). The expression of kinetic energy of rotary arm is described as

$$T_r = \frac{1}{2} J_r \left(\frac{d}{dt}\theta(t)\right)^2 \tag{6}$$

Similarly, the total potential energy, which is contributed by both elastic and gravitational energies, is expressed as

$$\begin{aligned} V = {} & m_{p1}\cos(\alpha(t)) + m_h g L_{p1}\cos(\alpha(t)) \\ & + m_{p2} g\{-\sin(\alpha(t)) l_{p2}\sin(\phi(t)) \\ & + \cos(\alpha(t)) l_{p2}\cos(\phi(t)) + l_{p1}\cos(\alpha(t))\} \end{aligned} \tag{7}$$

The matric form of the generalized coordinate vector q is derived as follows

$$D(q)\ddot{q} + C(q,\dot{q})\dot{q} + g(q) = \tau \tag{8}$$

Table 1. Quanser's rotary double inverted pendulum system specifications.

Parameters	Values	Units
Rotary arm mass, m_r	0.257	kg
Length of rotary arm, L_r	0.2159	m
Mass of pendulum 1, M_{p1}	0.257	kg
Moment of inertia for rotary arm, J_m	0.0041	kg m^2
Viscous damping of pendulum 1, B_{p1}	0.0024	N m s/rad
Length of center of mass from pivot point for pendulum 1, l_{p1}	0.1635	m
Pendulum 1 length, L_{p1}	0.2	m
Encoder hinge mass between two pendulum, m_h	0.1410	kg
Mass of pendulum 2, M_{p2}	0.127	kg
Viscous damping link 2, B_{p2}	0.0024	N m s/rad
Length of center of mass from pivot point for pendulum 2, l_{p2}	0.1778	m
Length of pendulum 2, L_{p2}	0.3365	m
Resolution of encoder, K_{enc}	4096	counts/rev

where, D, $g(q)$, and C represent inertial matrix, gravitational vector, and damping matrix, respectively. The required torque, τ generated by the servo motor to apply at the base of the rotary arm is given by the following equation

$$\tau = \frac{\eta_g K_g \eta_m k_t \left(V_m - K_g k_m \dot{\theta}\right)}{R_m} \tag{9}$$

The description and numerical values of the variables required to compute the motor torque are given by equation (9) and can be found in the work by Mehedi et al. (2018).

2.2. Model linearization

The linear state space model of RDIP system is described as

$$\begin{cases} \dot{x} = \mathcal{F}\mathbf{x} + \mathcal{G}V_m \\ y = \mathcal{H}\mathbf{x} \end{cases} \tag{10}$$

where $\mathbf{x} = \begin{bmatrix} \theta & \alpha & \phi & \dot{\theta} & \dot{\alpha} & \dot{\phi} \end{bmatrix}^T$ is the state variable vector, V_m is the controlled input voltage, and $\mathbf{y} = [\theta \quad \alpha \quad \phi]^T$ is the output vector of the linearized system. The control input voltage V_m should be maintained in such a way that the servo motor produces required torque that stabilizes the pendulum links with a minimum tolerable deflection angle. The functions $\mathcal{F}$, $\mathcal{G}$, and $\mathcal{H}$ represent the state transition, input, and output matrices, respectively, and are described as (Quanser, 2012)

$$\mathcal{F} = \frac{1}{J_T}\begin{bmatrix} 0 & 0 & 0 & 1 & 0 & 0 \\ 0 & 0 & 0 & 0 & 1 & 0 \\ 0 & 0 & 0 & 0 & 0 & 1 \\ 0 & a_a & -m_{p1} l_{p1} L_r m_{p2} g\left(-l_{p1} + L_{p1}\right) & 0 & 0 & 0 \\ 0 & a_b & \begin{matrix} -m_{p2} g\left(-L_r^2 L_{p1}\right) m_{p1} \\ + L_r^2 L_{p1} m_{p1} + J_r L_{p1} \end{matrix} & 0 & 0 & 0 \\ 0 & a_c & a_d & 0 & 0 & 0 \end{bmatrix} \tag{11}$$

$$\mathcal{G} = \frac{1}{J_T}\begin{bmatrix} 0 \\ 0 \\ 0 \\ M_h L_{p1}^2 + m_{p1} L_{p1}^2 \\ L_r\left(M_h L_{p1} + m_{p1} L_{p1}\right) \\ -\dfrac{L_r}{L_{p2}}\left(-m_{p1} L_{p1}^2 + m_{p1} L_{p1} L_{p2}\right. \\ \left. + M_h L_{p1} L_{p2} + m_{p1} L_{p1} L_{p1}\right) \end{bmatrix} \tag{12}$$

$$\mathcal{H} = [1 \quad 1 \quad 1 \quad 0 \quad 0 \quad 0] \tag{13}$$

The state transition and control input matrices, that is $\mathcal{F}$ and $\mathcal{G}$ of the linearized system are numerically represented by

$$\mathcal{F} = \begin{bmatrix} 0 & 0 & 0 & 1 & 0 & 0 \\ 0 & 0 & 0 & 0 & 1 & 0 \\ 0 & 0 & 0 & 0 & 0 & 1 \\ 0 & 368.1561 & -9.0635 & -1.1499 & 1.3285 & -1.4407 \\ 0 & 477.8131 & -40.7331 & -1.3285 & 1.8262 & -2.3306 \\ 0 & -518.1773 & 143.5827 & 1.4407 & -2.3306 & 4.1084 \end{bmatrix} \tag{14}$$

$$\mathcal{G} = \begin{bmatrix} 0 \\ 1 \\ 0 \\ 479.1375 \\ 553.5338 \\ -600.2946 \end{bmatrix} \tag{15}$$

3. RGDI control design

To stabilize two pendulum links at the upright position, while steering the fully actuated rotary arm at desired position or to follow certain reference command, RGDI control law is proposed which involves three stages. At the first stage, constraint differential equations are formulated based on the controlled-state variable deviation functions. In the second stage, for realizing the constraint differential equations, an equivalent control is designed, which is required for stable closed-loop performance. In the final stage, SMC-based discontinuous (switching) term is introduced in control law to compensate the impact of un-modeled dynamics, parametric uncertainties, and external perturbations followed by detailed stability analysis of closed-loop system using the Lyapunov candidate function.

3.1. Constraint dynamics

To represent the control objectives, time-varying differential equations of constraint dynamics are prescribed based on the error functions related to controlled state variables. The deviation functions of the state variables α, θ, and ϕ are expressed as

$$\zeta_\theta = \theta - \theta_d, \quad \zeta_\alpha = \alpha - \alpha_d, \quad \zeta_\phi = \phi - \phi_d$$

Based on the error function, three asymptotically stable time-varying constraint differential equations are constructed, whose order is same as that of state variables in terms of relative degree of control parameters, resulting in

$$\ddot{\zeta}_\theta + c_1\dot{\zeta}_\theta + c_2\zeta_\theta = 0 \tag{16}$$

$$\ddot{\zeta}_\alpha + c_3\dot{\zeta}_\alpha + c_4\zeta_\alpha = 0 \tag{17}$$

$$\ddot{\zeta}_\phi + c_5\dot{\zeta}_\phi + c_6\zeta_\phi = 0 \tag{18}$$

where the coefficients $c_1, c_2, \ldots c_6$ are selected appropriately around the equilibrium points, that is (ζ_θ, ζ_α, $\zeta_\phi = 0_{3\times1}$) (Hameduddin and Bajodah, 2012), so that the expressions given by equations (16)–(18) are asymptotically stable. By computing and placing the first and second time derivatives of error functions ζ_θ, ζ_α and ζ_ϕ in equations (16)–(18), resulting in the following algebraic system

$$\mathcal{A}V_m = \mathcal{B} \tag{19}$$

or

$$\begin{bmatrix} A_1 \\ A_2 \\ A_3 \end{bmatrix} V_m = \begin{bmatrix} B_1 \\ B_2 \\ B_3 \end{bmatrix} \tag{20}$$

where the elements of control vector coefficient function $\mathcal{A} : \mathbb{R}^n \times [t_0, \infty) \to \mathbb{R}^{3\times1}$ are given by

$$A_1 = \frac{1}{J_T}\left\{m_h L_{p1}^2 + m_{p1} L_{p1}^2\right\}$$

$$A_2 = \frac{1}{J_T}\left\{L_r\left(m_h L_{p1} + m_{p1} L_{p1}\right)\right\}$$

$$A_3 = \frac{1}{J_T}\left\{-\frac{L_r}{L_{p2}}\left(-m_{p1} L_{p1}^2 + m_{p1} L_{p1} L_{p2} + m_h L_{p1} L_{p2} + m_{p1} L_{p1}^2\right)\right\}$$

and the controls load function vector elements $\mathcal{B} : \mathbb{R}^n \times [t_0, \infty) \to \mathbb{R}^{3\times1}$ are inferred as

$$B_1 = \ddot{\theta}_d - F_{\dot{\theta}} - c_1\dot{\zeta}_\theta - c_2\zeta_\theta$$

$$B_2 = \ddot{\alpha}_d - F_{\dot{\alpha}} - c_3\dot{\zeta}_\alpha - c_4\zeta_\alpha$$

$$B_3 = \ddot{\phi}_d - F_{\dot{\phi}} - c_5\dot{\zeta}_\phi - c_6\zeta_\phi$$

where $F_{\dot{\theta}}$, $F_{\dot{\alpha}}$, and $F_{\dot{\phi}}$ are defined by the fourth, fifth, and sixth rows of equation (11).

3.2. Equivalent and switching control elements

The control effort required to stabilize the un-actuated pendulum links at vertically upward positions while keeping the actuated horizontal rotary arm at some arbitrary reference positions, and the proposed control law is stated by the following theorem

Theorem 1. Consider the closed loop system of RDIP system given by equation (10). The controlled state variables θ, α, and ϕ converge to zero in finite time, if the control voltage V_m given by equation (19) is expressed as

$$V_m = \overbrace{\mathcal{A}^+\mathcal{B}}^{V_{m_{eq}}} - \underbrace{\mathcal{A}^+\mathbf{K}\frac{\mathbf{s}}{\|\mathbf{s}\|}}_{V_{m_{rbt}}} \tag{21}$$

where $V_{m_{eq}}$ is the equivalent control controlled voltage realized by baseline GDI control approach and $V_{m_{rbt}}$ is the augmented switching control law based on the concept of SMC to provide robustness.

Proof. To realize the equivalent controlled voltage $V_{m_{eq}}$, the algebraic expression given by equation (19) is inverted using MPGI, which yields the following control law

$$V_{m_{eq}} = \mathcal{A}^{+}\mathcal{B} \tag{22}$$

where $\mathcal{A}^{+}$ is the MPGI of a tall vector function $\mathcal{A}$, described as

$$\mathcal{A}^{+} = \frac{\mathcal{A}^{T}}{\mathcal{A}^{T}\mathcal{A}} \tag{23}$$

To achieve the robust attributes, the augmentation of a discontinuous term with baseline GDI control is performed (Ansari et al., 2019b) to robustify the closed-loop performance against the influence of uncertain parameters, external disturbances, and system nonlinearities. The expression of resultant GDI–SMC or RGDI control law is given as

$$V_m = \mathcal{A}^{+}\mathcal{B} - \mathcal{A}^{+}\mathbf{K}\frac{\mathbf{s}}{\|\mathbf{s}\|} \tag{24}$$

where $\mathbf{K}$ is 3×3 positive gain matrix and $\|\cdot\|$ represents the Euclidean norm. The vector symbol $\mathbf{s}$ is the sliding surface vector which is computed by taking the time integral of the constraint differential equations given by equations (16)–(18), resulting in

$$\mathbf{s} = \begin{bmatrix} s_\theta \\ s_\alpha \\ s_\phi \end{bmatrix} = \begin{bmatrix} \dot{\zeta}_\theta + c_1\zeta_\theta + c_2\int\zeta_\theta \\ \dot{\zeta}_\alpha + c_3\zeta_\alpha + c_4\int\zeta_\alpha \\ \dot{\zeta}_\phi + c_5\zeta_\phi + c_6\int\zeta_\phi \end{bmatrix} \tag{25}$$

The controlled voltage V_m given by equation (24) comprised equivalent controlled voltage $V_{m_{eq}}$ that enforces the constraint dynamics and the switching term $V_{m_{rbt}}$ that enhances the robust attributes while improving the tracking performance.

3.3. Stability analysis

The time derivative of $\mathbf{s}$ is evaluated as

$$\dot{\mathbf{s}} = \begin{bmatrix} \dot{s}_\theta \\ \dot{s}_\alpha \\ \dot{s}_\phi \end{bmatrix} = \begin{bmatrix} \ddot{\zeta}_\theta + c_1\dot{\zeta}_\theta + c_2\zeta_\theta \\ \ddot{\zeta}_\alpha + c_3\dot{\zeta}_\alpha + c_4\zeta_\alpha \\ \ddot{\zeta}_\phi + c_5\dot{\zeta}_\phi + c_6\zeta_\phi \end{bmatrix} \tag{26}$$

Notice that asymptotic (or finite time) convergence of $\dot{s}$ to zero indicates asymptotic (or finite time) recognition of the constraint dynamics expressed by equations (16)–(18), and its algebraic equivalence is given by equation (19). Therefore

$$\dot{\mathbf{s}} = \mathcal{A}V_m - \mathcal{B} \tag{27}$$

To demonstrate the asymptotic convergence of the error mathematical model, the control law V_m expressed by equation (24) is used in the sliding mode formulations as given in equation (27), which results in

$$\begin{aligned} \dot{\mathbf{s}} &= \mathcal{A}\left\{\mathcal{A}^{+}\mathcal{B} - \mathcal{A}^{+}\mathbf{K}\frac{\mathbf{s}}{\|\mathbf{s}\|}\right\} - \mathcal{B} \\ &= \{\mathcal{A}\mathcal{A}^{+} - I_{3\times3}\}\mathcal{B} - \mathcal{A}^{+}\mathbf{K}\frac{\mathbf{s}}{\|\mathbf{s}\|} \end{aligned} \tag{28}$$

Now, positive definite Lyapunov candidate function is considered as follows

$$V = \frac{1}{2}\mathbf{s}^{T}\mathbf{s} \tag{29}$$

The time differentiation of V is computed as

$$\begin{aligned} \dot{V} = \mathbf{s}^{T}\dot{\mathbf{s}} &= \mathbf{s}^{T}\left\{(\mathcal{A}\mathcal{A}^{+} - I_{3\times3})\mathcal{B} - \mathcal{A}\mathcal{A}^{+}\mathcal{K}\frac{\mathbf{s}}{\|\mathbf{s}\|}\right\} \\ &= \mathbf{s}^{T}\{\mathcal{A}\mathcal{A}^{+} - I_{3\times3}\}\mathcal{B} - \mathbf{s}^{T}\mathcal{A}\mathcal{A}^{+}\mathcal{K}\frac{\mathbf{s}}{\|\mathbf{s}\|} \end{aligned} \tag{30}$$

The 2-(induced) norms of $\mathcal{A}\mathcal{A}^{+}$ and $\mathcal{A}\mathcal{A}^{+} - I_{3\times3}$ are both unity. It follows that $\dot{V} \leq 0$ is guaranteed if $\sigma_{\min}(\mathcal{K}) > \|\mathcal{B}(\mathbf{x}(0), 0)\|$, where $\sigma_{\min}$ is the minimum singular value function. Moreover, because $\dot{V} = 0$ occurs only at $\mathbf{s} = 0_3$, it follows from Lassale's principle (Khalil, 1996) that $\mathbf{s} = 0_3$ is attractive. Moreover, the discontinuous term in the right hand side of equation (30) implies that this condition on $\mathcal{K}$ guarantees finite time convergence of $\mathbf{s}$ and $\dot{\mathbf{s}}$ to the zero vectors, which implies asymptotic convergence of e_θ, e_α, and e_ϕ to zero. Finally, because it is assumed that the matrix gain $\mathcal{K}$ can be increased arbitrarily such that the stability condition is satisfied for any initial state condition, it follows that the design guarantees semi-global asymptotic stability of $(e_\theta, \dot{e}_\theta) = (e_\alpha, \dot{e}_\alpha) = (e_\phi, \dot{e}_\phi) = (0, 0, 0)$.

4. Controller validation

In this section, the tracking performance and stability test of RGDI control law are demonstrated through computer simulations and real-time experiments on the RDIP system. Numerical simulations are performed on the linearized dynamic model of RDIP given by equation (10), whereas the real-time experiments are executed on Quanser's RDIP test bed.

4.1. Numerical simulation

In this section, a simulation environment is created in Simulink/MATLAB, in which a reference sinusoidal signal is commanded to the rotary arm whose expression is given by

$$\theta_d = \pm 30\sin(2\pi 0.05t) \tag{31}$$

While tracking the sinusoidal trajectory, the controller maintains the angular displacement of α and ϕ of two pendulum links at the upright position, that is $\phi = 0$ and $\alpha = 0$. The initial values of the state vector is defined as

$$\begin{bmatrix} \theta & \alpha & \phi & \dot{\theta} & \dot{\alpha} & \dot{\phi} \end{bmatrix} = \begin{bmatrix} 0 & 0 & 0 & 0 & 0 & 0 \end{bmatrix} \quad (32)$$

In addition, the performance of RGDI control is being compared with the state-of-the-art SMC and with conventional GDI system (eliminating the SMC based switching term). Furthermore, ±20% random variations in numerical values of mass, length, moment of inertia, and other parameters of RDIP system are considered to verify robust characteristics. The time response curves of controlled state variables and control efforts for three control methodologies are shown in Figure 2. The rotary arm angular position tracking is visualized in Figure 2(a), which reveals that the RGDI control demonstrates smooth performance and faster convergence towards the reference command as than the SMC and GDI control approaches. The angular positions α and ϕ of the two pendulum links are shown in Figure 2(b) and (c), respectively. It is observed that the RGDI control effectively kept both pendulum links at the upright position with little oscillations, as compared with SMC whose response curves depict higher fluctuations. The controlled voltages generated by the three control strategies required to stabilize the RDIP system are plotted in Figure 2(d).

4.2. Experimental setup

To examine the real-time performance, the proposed controller is implemented on Quanser's RDIP practical test bench, whose experimental setup is shown in Figure 3. The experimental setup comprised voltage amplifier VoltPAQ-X1 that transmit voltage to Quanser SRV02 servo motor that actuates the horizontal rotary arm, which in turn creates the angular motions of double inverted pendulums. The expressions of two components of RGDI control, that is equivalent control $V_{m_{eq}}$ and switching control $V_{m_{rbt}}$ are implemented in MATLAB Simulink environment. The Simulink modules communicate with the real RDIP practical test bench via Quanser real-time control, an state-of-the-art rapid prototyping and production system used for real-time control. It integrates smoothly with Simulink through which the Simulink models are executed in real time on variety of targets. The angular position feedbacks are sent to the computer via data acquisition board Quanser's Q8-USB that acts as an interface between the hardware and software. To commence the experiment, the RDIP system is activated by lifting both pendulum arms

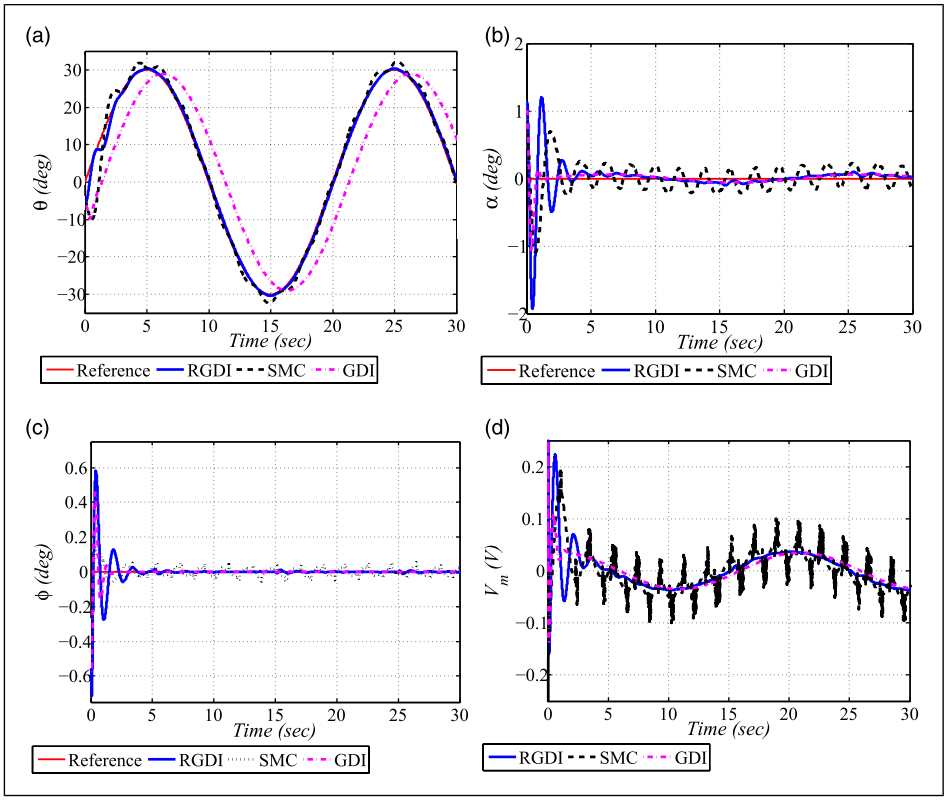

Figure 2. Computer simulations: sine-wave tracking; (a) angular displacement of rotary arm, (b) pendulum angle: lower link, (c) pendulum angle: upper link, and (d) controlled voltage.

manually to the vertical equilibrium position (near zero). During experiments, the initial time interval is overlooked which was consumed to manually erect the double pendulum links close to the vicinity of the equilibrium point.

4.3. Stabilization problem

In this experiment, stabilization problem is addressed through RGDI control by maintaining the rotary arm at zero position while keeping and balancing the double inverted pendulum links at the upright position. Furthermore, random variations of ±20% are also made in the magnitude of RDIP system parameters to visualize how these variations could impact the controller's performance. For comparative analysis, the experimental results of RGDI are also compared with classical SMC and FOC strategies. The evolution of three controlled state variables, that is θ, α, and ϕ as well as the applied control voltages are illustrated in Figure 4. The time histories of the rotary arm angular position tracking is shown in Figure 4(a), which reveals that the RGDI control exhibits better time domain performance by keeping the rotary arm close to reference command as compared with the SMC and FOC laws. For the case of FOC, the rotary arm keep fluctuating around ±8° over the complete time interval without attenuation. Similar trends have been observed in the angular positions of the two pendulum links α and ϕ for the case of FOC as shown in Figure 4(b) and (c), respectively. The pendulum angles α and ϕ are oscillating in the band of approximately 10° caused by FOC, whereas the band shrinks to 5° when RGDI and SMC laws are applied. However, although the pendulum angles fluctuate, all the three methods are capable to stabilize the RDIP system. The time histories of the generated controlled voltages by three control methods are observed in Figure 4(d), which are well under the saturation limits.

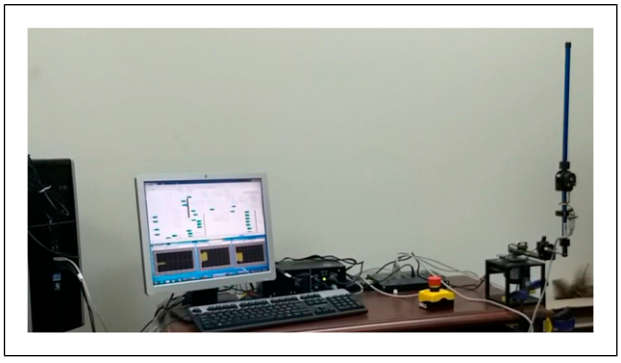

Figure 3. Experimental setup for robust generalized dynamic inversion implementation.

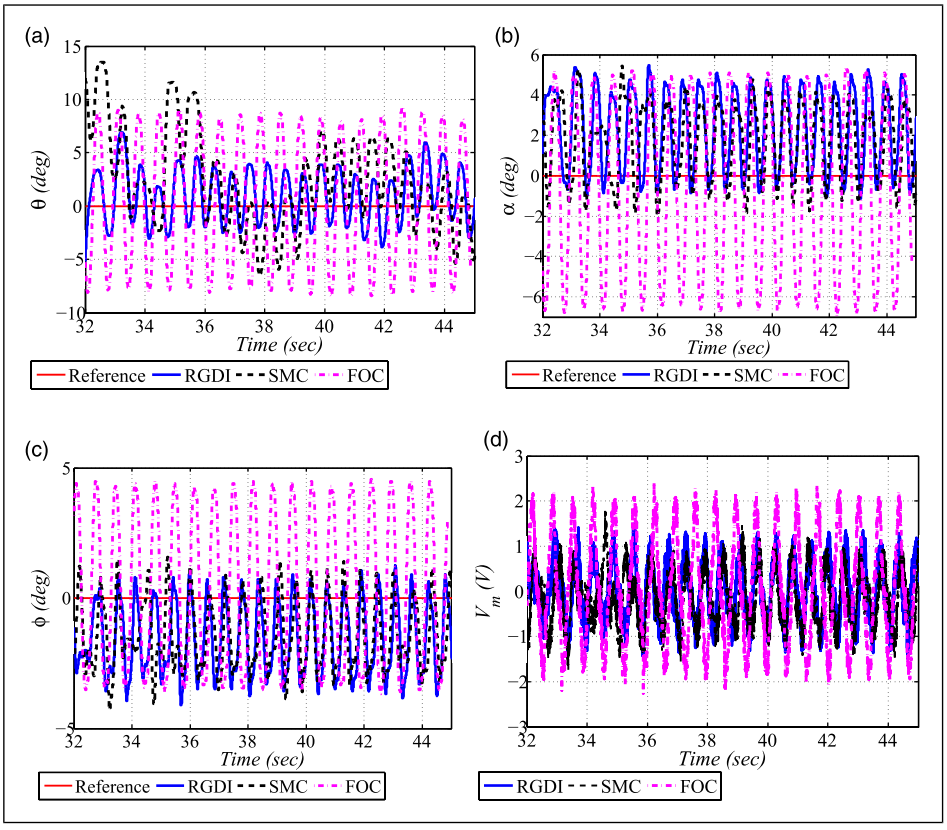

Figure 4. Experimental results: stabilization problem; (a) rotary arm displacement, (b) pendulum angle: lower link, (c) pendulum angle: upper link, and (d) required controlled voltage.

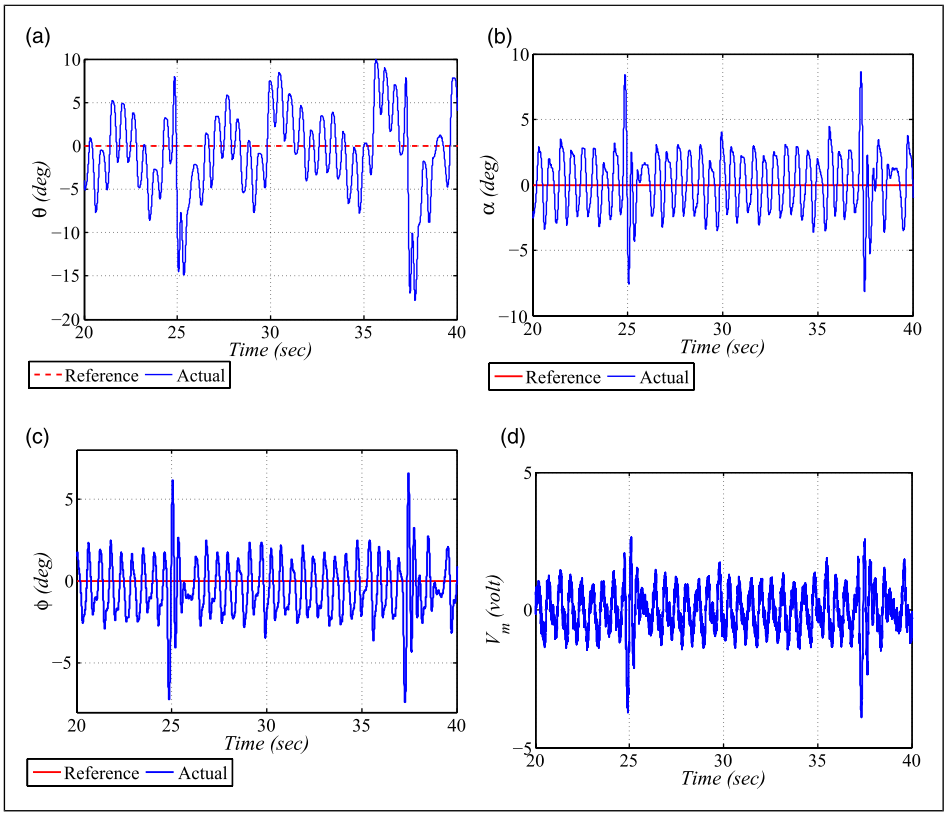

Figure 5. Experimental results: disturbance rejection; (a) rotary arm displacement, (b) pendulum angle: lower link, (c) pendulum angle: upper link, and (d) controlled voltage.

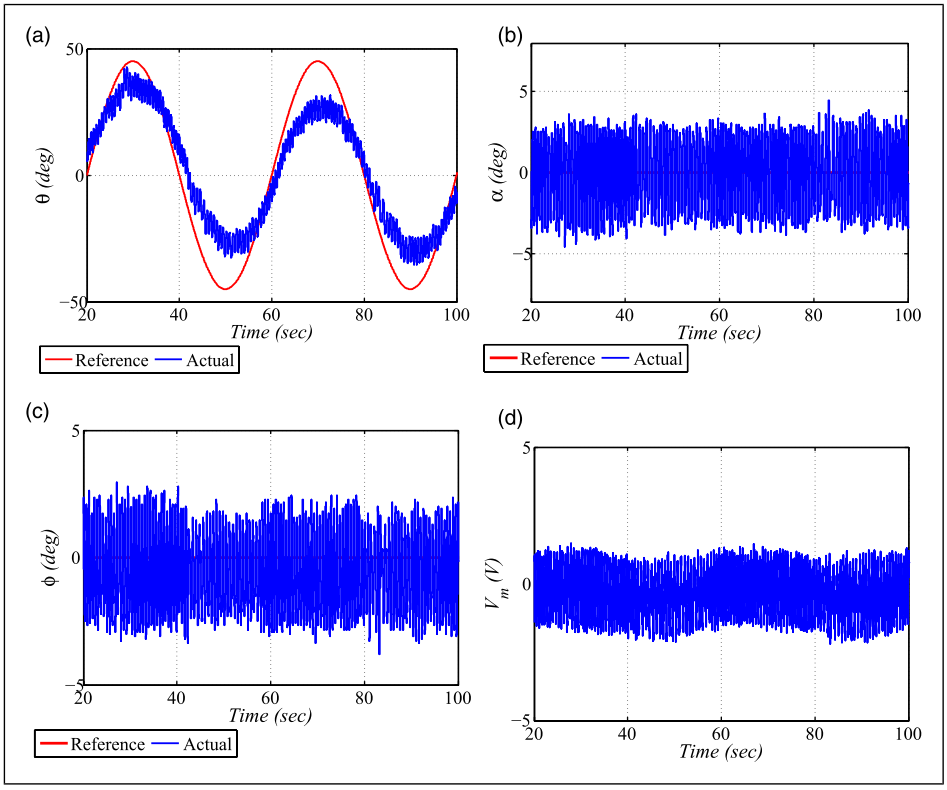

Figure 6. Experimental results: sine-wave tracking; (a) rotary arm displacement (b) pendulum angle: lower link, (c) pendulum angle: upper link, and (d) controlled voltage.

4.4. Disturbance rejection capability

The disturbance rejection capability is demonstrated in this section by manually tapping the upper pendulum link. The upper pendulum link is tapped lightly at time instants 25 s and 37 s, which in turn changes the pendulum angular positions α and ϕ. The experimental results under the effect of manual disturbance are shown in Figure 5. Because of applied disturbance, the top and bottom pendulums are distorted and tend to oscillate; however, the controller reacts immediately and re-stabilize both pendulums towards its stable upright position. The snapshots of the three angular positions, that is θ, α, and ϕ are illustrated in Figure 5(a)–(c), respectively. The controlled voltage also fluctuates with applied disturbances, but its magnitude is still under the supplied capacity, whose time response is depicted in Figure 5(d).

4.5. Sine-wave tracking

To investigate further, a reference sinusoidal profile is commanded to the horizontal rotary arm, whose kinematical equation is described as

$$\theta_d = \pm 45 \sin(2\pi 0.025t) \tag{33}$$

The key performance indices that include θ, α, ϕ, and V_m are illustrated in Figure 6. The sinusoidal angular pattern followed by the rotary arm is shown in Figure 6(a). The result depicts smooth convergence plot towards the reference trajectory while stabilizing the top and bottom pendulum links at the upright position whose time domain curves are demonstrated in Figure 6(b) and (c), respectively. The corresponding controlled voltage required to stabilize the RDIP system is shown in Figure 6(d), which is well under the saturation limit.

5. Conclusion

Stabilization and tracking performance of an RDIP system has been successfully evaluated in this article by using the RGDI control methodology. MPGI-based constraint dynamics are realized by this control law which tracks the angular position of the rotary arm and at the same time, it keeps both the pendulum links (upper and lower) in the upright positions. SMC-based discontinuous element is incorporated to robustify the closed-loop performance against system uncertainties, nonlinearities, and external disturbances. The resultant control law guarantees semi-global asymptotically stable tracking performance. Computer simulations are conducted to visualize the pre-experimental performance of RGDI control, followed by experimental investigations and detailed comparative analysis with SMC and FOC methodologies.

Acknowledgement

This work was supported by the Deanship of Scientific Research (DSR), King Abdulaziz University, Jeddah, under grant No. (DF-250-135-1441). The authors, therefore, gratefully acknowledge DSR technical and financial support.

Declaration of conflicting interests

The author(s) declared no potential conflicts of interest with respect to the research, authorship, and/or publication of this article.

Funding

The authors received financial support for the research from King Abdulaziz University, Jeddah.

ORCID iD

Ibrahim M Mehedi https://orcid.org/0000-0001-8073-9750

References

Ansari U and Bajodah AH (2017) Robust launch vehicle's generalized dynamic inversion attitude control. *Aircraft Engineering and Aerospace Technology* 89(6): 902–910.

Ansari U and Bajodah AH (2018a) Quadrotor motion control using adaptive generalized dynamic inversion. In: Annual American control conference (ACC), WI, USA, 27–29 June 2018, pp. 4311–4316. USA: IEEE.

Ansari U and Bajodah AH (2018b) Robust generalized dynamic inversion based control of autonomous underwater vehicles. *Proceedings of the Institution of Mechanical Engineers, Part M: Journal of Engineering for the Maritime Environment* 232(4): 434–447.

Ansari U and Bajodah AH (2019) Launch vehicle ascent flight attitude control using direct adaptive generalized dynamic inversion. *Proceedings of the Institution of Mechanical Engineers, Part G: Journal of Aerospace Engineering* 233(11): 4141–4153.

Ansari U, Bajodah AH and Hamayun MT (2019a) Quadrotor control via robust generalized dynamic inversion and adaptive non-singular terminal sliding mode. *Asian Journal of Control* 21(3): 1237–1249.

Ansari U, Bajodah AH and Kada B (2019b) Development and experimental investigation of a quadrotor's robust generalized dynamic inversion control system. *Nonlinear Dynamics* 96(2): 1541–1557.

Ansari U, Bajodah HA and Alam S (2018) Adaptive generalized dynamic inversion based trajectory tracking control of autonomous underwater vehicle. In: 26th Mediterranean conference on control and automation (MED), Zadar, Croatia, 19–22 June 2018, pp. 1–9. USA: IEEE.

Dabiri A, Nazari M and Butcher EA (2016) Linguistic fuzzy logic control of a double inverted pendulum with destabilizing fractional dampers. In: ASME 2016 international mechanical engineering congress and exposition, Phoenix, AZ, 11–17 November 2016. USA: American Society of Mechanical Engineers Digital Collection.

Hameduddin I and Bajodah AH (2012) Nonlinear generalised dynamic inversion for aircraft manoeuvring control. *International Journal of Control* 85(4): 437–450.

Hoang H and Wongsaisuwan M (2007) Robust controller design for a rotary double inverted pendulum using linear matrix inequalities. In: SICE annual conference 2007, Takamatsu, Japan, 17–20 September 2007, pp. 515–520. USA: IEEE.

Jabbar A, Malik FM and Sheikh SA (2017) Nonlinear stabilizing control of a rotary double inverted pendulum: a modified backstepping approach. *Transactions of the Institute of Measurement and Control* 39(11): 1721–1734.

Khalil HK (1996) *Nonlinear Systems*. New Jersey: Prentice-Hall.

Mehedi IM, Al-Saggaf UM, Mansouri R, et al. (2019) Stabilization of a double inverted rotary pendulum through fractional order integral control scheme. *International Journal of Advanced Robotic Systems* 16(4): 1729881419846741.

Mehedi IM, Ansari U, Bajodah AH, et al. (2018) Positional control of rotary servo cart system using generalized dynamic inversion. *Journal of Vibroengineering* 20(6): 2403–2413.

Moore EH (1920) On the reciprocal of the general algebraic matrix. *Bulletin of American Mathematical Society* 26: 394–395.

Nejadfard A, Yazdanpanah MJ and Hassanzadeh I (2013) Friction compensation of double inverted pendulum on a cart using locally linear neuro-fuzzy model. *Neural Computing and Applications* 22(2): 337–347.

Patil M and Kurode S (2017) Stabilization of rotary double inverted pendulum using higher order sliding modes. In: 2017 11th Asian control conference (ASCC), Queensland, Australia, 17–20 December 2017, pp. 1818–1823. USA: IEEE.

Penrose R (1955) A generalized inverse for matrices. *Mathematical proceedings of the Cambridge philosophical society* 51: 406–413.

Quanser (2009) *Quanser SRV02 User Manual.* Canada: Quanser Inc.

Quanser (2012) *Quanser Innovative Edutech Laboratory Guide - Rotary Double Inverted Pendulum Experiment.* Canada: Quanser Inc.

Singh N and Yadav SK (2012) Comparison of lqr and pd controller for stabilizing double inverted pendulum system. *International Journal of Engineering Research and Development* 1(12): 69–74.

Yadav SK, Sharma S and Singh N (2012) Optimal control of double inverted pendulum using lqr controller. *International Journal of Advanced Research in Computer Science and Software Engineering* 2(2): 189–192.

Young A, Cao C, Hovakimyan N, et al. (2006) Control of a nonaffine double-pendulum system via dynamic inversion and time-scale separation. In: 2006 American control conference, MN, USA, 14–16 June 2006, pp. 6. USA: IEEE.